Effects of Coulomb collisions in solid-density laser plasma shocks

A. Sundström[1], E. Siminos[2], L. Gremillet[3], I. Pusztai[1]

[1] *Department of Physics, Chalmers University of Technology, 412 96 Göteborg, Sweden*

[2] *Department of Physics, Gothenburg University, 412 96 Göteborg, Sweden*

[3] *CEA, DAM, DIF, F-91297 Arpajon, France*

Using particle-in-cell (PIC) simulations, we numerically investigate the processes of bulk electron heating and ion acceleration in high-Z^*, solid-density, sub-micron targets irradiated by high-intensity ($I \approx 5\times10^{20}\,\mathrm{Wcm^{-2}}$), femtosecond laser pulses, either linearly or circularly polarized. Using a high-Z^* ion species at high density increases the effect of Coulomb collisions on the plasma dynamics. In sub-micron targets, collisional energy absorption through an inverse Bremsstrahlung (IB) type effect dominates the bulk electron heating, thus both linear and circular laser polarizations result in similar bulk electron temperatures. These results are of interest for the experimental generation of high energy density (HED) matter samples. Due to the higher electron temperature in the collisional case, an electrostatic shock is observed to form.

Simulation parameters We use the Smilei PIC code [1], which has a relativistic binary collision module [2]. All quantities, unless otherwise specified, are normalized to the Smilei base units: laser frequency ω, electron mass m_e, elementary charge e, and the speed of light c; densities are given in the critical density $n_\mathrm{c} = \varepsilon_0 m_\mathrm{e}\omega^2/e^2$, where ε_0 is the vacuum permittivity.

We perform 1D simulations in a box of size 20 µm with a resolution of $\Delta x = 0.39\,\mathrm{nm}$ (51200 cells) for a simulation time of 120 fs. We consider both linearly (LP) and circularly (CP) polarized lasers with wavelength 0.8 µm, dimensionless amplitude $a_0 = 15$ (i.e., an intensity of $I = \frac{c\varepsilon_0}{2}(\frac{m_\mathrm{e}c\omega a_0}{e})^2 \approx 5\times10^{20}\,\mathrm{Wcm^{-2}}$), and a Gaussian temporal profile with 10 fs full-width-half-maximum duration. The plasma is 300 nm thick, starting at $x = 1.0\,\mu\mathrm{m}$, consisting of an equal mixture of protons and Cs^{27+} ions, such that $n_{0,\mathrm{e}} = 250\,n_\mathrm{c}$ (the skin depth $l_\mathrm{s} = 8.0\,\mathrm{nm}$ is resolved), with 500 macro-particles per species per cell; the particles are initially distributed as Maxwellians with temperatures $T_{\mathrm{e},0} = 1\,\mathrm{eV}$ for the electrons and $T_{\mathrm{i},0} = 0.1\,\mathrm{eV}$ for the ions.

Collisional electron heating For both LP and CP pulses, Fig. 1 shows that, at the time of the laser peak ($t = 21.1\,\mathrm{fs}$), the collisionless and collisional simulations both reach similar maximum electron energies ($\sim 200\,\mathrm{keV}$). Moreover, both CP and LP achieve similar high-energy spectra, which indicates that the electron energy is then mainly associated with transverse momentum in the laser field. In the collisionless CP case, however, the electrons cannot retain that high energy after the pulse has passed ($t = 58.6\,\mathrm{fs}$). This means that, with collisions enabled, the electrons are dominantly heated collisionally by an IB type mechanism. The electron collisional

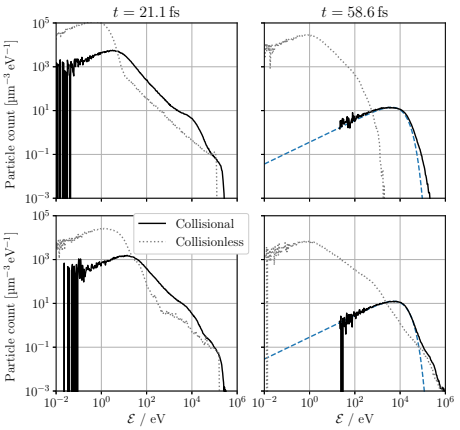

Figure 1: *Electron energy spectra at peak laser intensity (left) and well after the pulse has passed (right), using CP (top) and LP (bottom). Dashed blue lines show fitted Maxwellians, which in both cases have a temperature of* 10 keV. *During the pulse, both the collisional and collisionless spectra are fairly similar. After the pulse, however, the collisional spectra has retained much more of the electron energy. Both with and without collisions, the two LP spectra retain a long-lived high-energy tail up to* $\mathcal{E} \sim 3$ MeV *(beyond the truncation of the figure).*

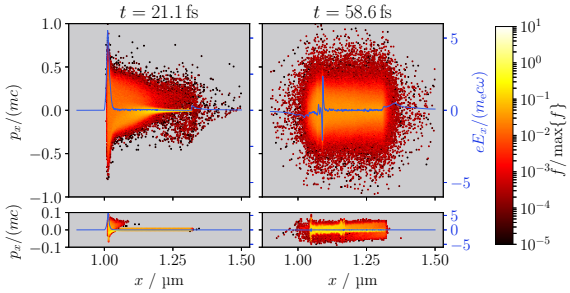

Figure 2: *Electron distributions at (left) and well after the laser peak intensity (right), with (top) and without (bottom) collisions, using CP. With collisions, the electrons reach* ∼10 *times larger longitudinal momenta* p_x *than without. Blue curve: longitudinal electric field* E_x.

mean free path, $\lambda_{\mathrm{mfp}} \sim 10-100$ nm, is comparable to the skin depth $l_s = 8$ nm, which suggests that the heating may also be influenced by the normal and anomalous skin effects [3].

In these targets, the collisional electron bulk is heated to $T_e \approx 10$ keV with both CP and LP, as seen in Fig. 1 ($t = 58.6$ fs). Using CP, the electron population is thermalized in ∼20 fs after the pulse. In the case of LP, both collisional and collisionless electrons are energized through a vacuum heating [4] type mechanism up to an energy of $\mathcal{E} \sim 3$ MeV. This high-energy tail is long-lived (∼100 fs), even with collisions, and can interfere in, e.g., HED atomic physics studies.

Electron distribution When studying the electron $x-p_x$ phase-space distribution (with CP), shown in Fig. 2, the strong collisional heating becomes apparent. Electrons in the skin layer ($x \approx 1$ µm) are first energized in the transverse plane by the laser electric field. In the collisionless case, the electrons acquire longitudinal momentum mainly due to the ponderomotive force associated with the rapid rise of the laser profile. By contrast, in the collisional case, the transverse electron momenta are efficiently scattered into the longitudinal direction, quickly leading to an isotropic, well-homogenized hot electron distribution. This effect is self-sustained: the slight expansion of the target front caused during the interaction by the much increased electron p_x leads to an enhanced local laser field, and therefore an increased electron energization.

Proton and Cs-ion distributions Initially, radiation pressure is strong enough to accelerate the Cs ions and protons to twice the hole-boring velocity $2v_{\mathrm{HB}} \approx 2ca_0[Z^* m_e n_c/(m_{\mathrm{Cs}} n_e)]^{1/2} \sim 0.02c$, independently of collisions; the charge separation field underpinning this acceleration is clearly visible in the $t = 21.1$ fs panels of Fig. 3. The large electron thermal spread at the laser piston

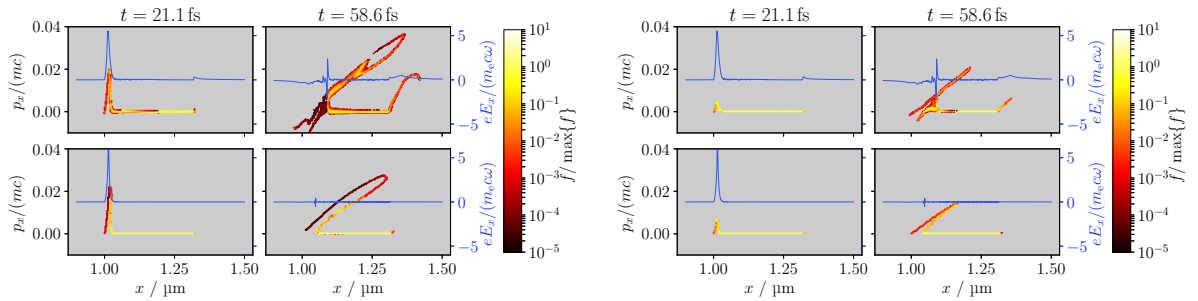

Figure 3: *Proton (left) and Cs-ion (right) distributions at peak laser intensity ($t = 21.1\,\mathrm{fs}$) and after the pulse has passed ($t = 58.5\,\mathrm{fs}$), with (top) and without (bottom) collisions, using CP. The longitudinal electric field (blue) initially represents a charge separation layer due to radiation pressure; at the later time, an electrostatic shock has developed in the collisional case.*

(upper left panel in Fig. 2), corresponds to an electron temperature of $T_\mathrm{e} \sim 100\,\mathrm{keV}$ and thus an ion acoustic sound speed of around $c_\mathrm{s} \approx (T_\mathrm{e} Z^*/m_\mathrm{Cs})^{1/2} \sim 0.005c$. The radiation pressure piston is therefore moving with a Mach number $\mathcal{M} \sim 2$, which fulfills the standard shock formation condition $1.6 \lesssim \mathcal{M} \lesssim 3.5$ [5]. We also see evidence of a shock in the oscillations of the longitudinal electric field, E_x, and in the modulations of ion distributions behind the acceleration front. The heavy Cs ions are responsible for sustaining the electrostatic shock potential; while only a minority of them is reflected by the shock, almost all protons are reflected due to their larger charge-to-mass ratio [6]. In the collisionless case, on the other hand, the electron temperature is not high enough to sustain a shock moving at the piston velocity; thus the field quickly decays, no shock is formed, and the accelerated ion energy decreases faster than in the collisional case.

A more direct effect of collisions on the ion distributions is the broadening in p_x of the reflected proton population, which corresponds to a proton temperature of $T_\mathrm{p} \sim 1\text{–}10\,\mathrm{keV}$, as seen in Fig. 3. This effect is present in both CP and LP. Simulations with either $\mathrm{p}^+\text{–}\mathrm{Cs}^{27+}$ or $\mathrm{p}^+\text{–}\mathrm{e}^-$ collisions disabled show that collisional friction between the protons and the Cs-ions is responsible for this ion heating. However, this result differs from the "ultra fast collisional ion heating" reported by Turrell et al. [7]. Despite considering almost identical simulation parameters, these authors found that the friction due to $\mathrm{p}^+\text{–}\mathrm{Cs}^{27+}$ collisions completely suppressed proton reflection on sub-fs time scales, and induced strong proton heating in the downstream. Our simulations indeed show a friction-induced heating of the protons, but (i) it concerns the *reflected* population only; and (ii) this heating occurs on a $\sim$10 fs time scale. We suspect that this discrepancy might be due to a faulty collision module in the version of the code used in [7].

Simplified absorption model We have performed simulations of a simplified scenario to elucidate the collisional electron heating mechanism in CP. The scenario consists of a semi-infinite plasma of the same composition and density as the main simulations, but with immobile ions and a constant laser intensity after a linear ramp-up. We study the quasi-steady state reached

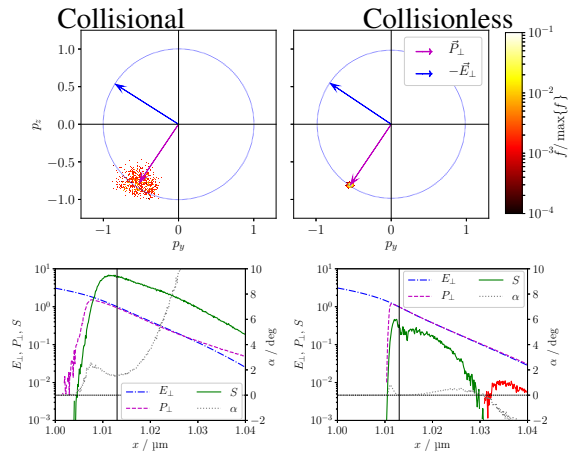

Figure 4: *Top: Transverse electron momentum distribution inside the skin layer in relation to the local electric field; arrows show the transverse electric field $\vec{E}_\perp$ and momentum moment $\vec{P}_\perp$ vectors. Bottom: Magnitude of the transverse electric field $E_\perp$ and momentum moment $P_\perp$, as well as absorbed power density S (green indicates $S > 0$, red is $S < 0$), and phase shift angle α; values are averaged over a duration of* 10 fs. *Vertical lines denote the location of the top distributions.*

after an initial transient: the laser field $\vec{E}_\perp(x)$ and the transverse momentum moment of the electron distribution $\vec{P}_\perp(x)$ co-rotate in the transverse momentum plane (top panels of Fig. 4). Without collisions, $\vec{P}_\perp$ and $\vec{E}_\perp$ stay perpendicular to each other. However, collisions spread out the electron distribution and cause a phase shift in $\vec{P}_\perp$, so that the angle between $\vec{P}_\perp$ and $-\vec{E}_\perp$ becomes $90^\circ - \alpha$, with $\alpha > 0$. The power absorption density from the laser electric field is $S = -n_e \vec{V}_\perp \cdot \vec{E}_\perp = n_e V_\perp E_\perp \sin(\alpha)$, where $\vec{V}_\perp$ is the perpendicular velocity moment of the electron distribution; thus the collisionally induced phase shift causes a net laser energy absorption.

In the bottom panels of Fig. 4, we see that $\alpha \approx 1^\circ - 2^\circ$ throughout the skin layer of the collisional simulation, while the collisionless simulation only produces $\alpha \sim 0.05^\circ$ in the same region; consequently, S is about $1-2$ orders of magnitude smaller without collisions. The conservation of canonical momentum requires that $P_\perp = E_\perp$ (in this normalization). However, the left panels of Fig. 4 show that collisions also reduce the magnitude of the electron transverse momentum; this "missing" transverse momentum has gone into the ions.

Conclusions An inverse Bremsstrahlung type effect causes significant energy absorption in high-Z^*, sub-micron, solid targets comprising a mixture of high-Z^* ions and protons, driven by $5 \times 10^{20}\,\mathrm{Wcm}^{-2}$, 10 fs laser pulses. Energy absorption takes place through a collisionally induced phase shift between the transverse electron momentum and the laser electric field. The targets reach a bulk electron temperature of 10 keV, corresponding to an energy density of $10^9\,\mathrm{J/cm}^3$. With circular polarization, the whole electron distribution thermalizes very rapidly, which makes it interesting for high energy density studies. Without collisions, the electrons do not attain temperatures high enough to form a shock as a result of the laser-induced piston.

References

[1] J. Derouillat, et al. *Comput. Phys. Commun.*, **222**:351 (2018).

[2] F. Pérez, et al. *Phys. of Plasmas*, **19**:083 104 (2012).

[3] W. Rozmus, et al. *Phys. Rev. A*, **42**:7401 (1990).

[4] J. May, et al. *Phys. Rev. E*, **84**:025 401 (2011).

[5] D. W. Forslund, et al. *Phys. Rev. Lett.*, **25**:1699 (1970).

[6] I. Pusztai, et al. *Plasma Phys. Control. Fusion*, **60**:035 004 (2018).

[7] A. E. Turrell, et al. *Nat. Commun.*, **6**:8905 (2015).